The Effects of Confining Pressure and Stress Difference on Static Fatigue of Granite

ROBERT L. KRANZ

Department of Geological Sciences and
Lamont-Doherty Geological Observatory
of Columbia University, Palisades, NY 10964

ABSTRACT

Samples of Barre granite were creep tested at room temperature at confining pressures up to 2 kilobars. The time to fracture increased with decreasing stress difference at every pressure, but the rate of change of fracture time with respect to the stress difference increased with pressure. At 87% of the short-term fracture strength, the time to fracture increased from about 4 minutes at atmospheric pressure to longer than one day at 2 Kb of pressure. The inelastic volumetric strain at the onset of tertiary creep, Δ, was constant within 25% at any particular pressure but increased with pressure in a manner analogous to the increase of strength with pressure. At the onset of tertiary creep, the number of cracks and their average length increased with pressure. The crack angle and crack length spectra were quite similar, however, at each pressure at the onset of tertiary creep.

6971

Lamont-Doherty Geological Observatory Contribution No. 0000

Several theories of static fatigue are all found to adequately explain the data. They suggest that the activation enthalpy for the stress corrosion process which controls the creep rate increases with pressure. The creep strains are best fit by power functions of both stress and time. Risking the extrapolation to longer times, the data suggest that creep rupture in the upper crust is possible only if deviatoric stresses of several kilobars can be maintained for millions of years, if substantial pore pressures can lower the effective pressure, or if temperature substantially increases the rate of stress corrosion.

INTRODUCTION

The effects of mechanical, chemical and structural variables on the fracture strength of rock are well known, having been studied together and separately to a great extent. The effects of many of these on the time-dependent deformation of rock are less well known. In particular, the effect of external or confining pressure on static fatigue and creep rupture has not been systematically investigated independently of the other variables.

The problem of the pressure effect on static fatigue is most important in the upper crust, becoming subsidiary to temperature effects with increasing depth. The transition depth, where creep rupture is no longer possible owing to increasing ductility, is unknown. It is significant that dilatancy caused by microfracturing occurs in crystalline rock at pressures up to 8 Kb [Brace et al., 1966] and temperatures up to 400°C [Hadley, 1975a]. Microcracks can coalesce to produce macrofractures in granite at P-T conditions at least up to 5 Kb and 400°C [Tullis and Yund, 1977]. Unrealistically high differential stresses are required at these pressures, however, unless static fatigue, by whatever mechanism, has lowered rock strength.

Early work on this problem by Griggs [1936, 1939], and Robertson [1960] on limestone, gypsum and marble concentrated only on transient creep where the creep rate persistently decreases. In this stage, strain appeared to be proportional to the logarithm of time under load, but the proportionality factor was a function of the applied stress

difference (maximum stress minus confining pressure). Increasing the confining pressure decreased the creep rate while increasing the maximum stress, at any particular pressure, increased the creep rate. The data indicated a change in the mechanism responsible for static fatigue from dominantly microfracturing below 2 kilobars to some combination of ductile and brittle deformation at higher pressures. Most of these tests were performed with loads that were periodically incremented so the effect of sustained stress difference was mixed with the effects of strain history.

A large number of uniaxial creep tests (confining pressure equal to one atmosphere) have been performed on the silicates, but even now few data exist at higher pressures. Most of these are for high temperature tests where primary interest is centered on steady-state flow; for reviews see Carter and Kirby [1978] and Heard [1976]. In this regime, the strain rate is nearly constant and is usually described by an Arrhenius type equation where the proportionality constant is in fact a function of stress. The functional form is usually given as the stress difference raised to some power.

The middle ground, from room temperature and pressure to those relevant to the upper crust, is almost barren. Williams and Elizzi [1976] have tested gypsum at a constant maximum stress of 400 bars, varying confining pressure from 1 to 300 bars. Cogan [1976] has tested limestone and shale at low axial loads and pressures up to about 40 bars. The most complete data come from Wawersik and Brown [1973] and

Wawersik [1972] who tested a granite and sandstone at pressures of 70, 350 and 690 bars pressure at room temperature. Creep rupture at these pressures was observed in only four experiments. Pressure decreased both the primary and secondary strain rates at all stress differences employed. Strain was described as proportional to a power function of time under load with the exponent less than unity.

It is apparent that pressure acts to inhibit creep deformation and will increase the time taken to initiate rupture if all other factors are constant. Is there a relationship between the pressure effect on the short-term strength of rock and its effect on static fatigue? How do we account for the pressure effect in existing creep equations and theories of static fatigue? With the answers to these questions as its goal, an experimental program was initiated several years ago to examine both the microscopic and macroscopic effects of pressure and stress difference. The current results are given in this paper.

EXPERIMENTAL PROCEDURE

By preparing and testing one rock type (in this investigation, Barre granite) in a consistent manner, most of the effects of strength factors other than pressure and stress difference can be neutralized. All samples were cored from two separate blocks in a direction perpendicular to the rift plane. Block A was the same block used by Kranz and Scholz [1977] for their uniaxial experiments; their results will

be incorporated within this report. Samples from the two blocks had nearly the same pressure dependent fracture strength. Grain size, initial crack density and bulk compressibility were similar. Thus variability attributable to using separate blocks is discounted.

Cores were right circular cylinders, 3.46 ± .02 cm in diameter and 8.9 ± .1 cm in length. They were soaked in acetone and dried under ambient laboratory conditions. Several days before testing they were jacketed with thin copper. Electrical resistance strain gauges with effective gauge lengths of both 1.27 cm and 2.54 cm were cemented to the jackets without regard to any specific preferred crack orientation within the sample. Gauges were aligned to measure strain parallel (ε_z) and perpendicular (ε_r) to the cylinder axis.

Volumetric strain ($\Delta V/V$) was determined in three ways. The parallel and two perpendicular gauges were connected directly on the jacket; the output was assumed to be proportional to the volumetric strain. In addition, the individual outputs from two separate parallel and perpendicular gauges were externally added electronically to measure the volumetric strain. Under stress, rock deforms anisotropically, especially while dilating [Hadley, 1975b] and these two supposedly redundant methods often gave different results. Therefore an additional averaging technique was employed. Because the initially circular cross section becomes progressively more elliptical, where possible the principal strains perpendicular to the cylinder axis were determined. Instead of using $\Delta V/V = 2\varepsilon_r + \varepsilon_z$ volumetric strain was

calculated using $\Delta V/V = \varepsilon_{r1} + \varepsilon_{r2} + \varepsilon_z$, where ε_{r1} and ε_{r2} are the principal strains of the plane perpendicular to the z axis of the cylinder.

Experimentally, the horizontal 2.54 cm gauge intended to record circumferential strain, gave a value somewhere between the two radial principal strains, usually near the maximum, so that volumetric strain calculated using it was too high. Volumetric strain from the 1.27 cm gauges connected on the sample gave a value close to that calculated using the principal strains, probably because the effective gauge length of this configuration covers more than half the sample circumference. Both ε_r and ε_z from the 2.54 cm gauges as well as $\Delta V/V$ from the 1.27 cm gauge configuration are reported. Strains are given with respect to the pre-load, hydrostatic state.

Excepting the uniaxial tests of Kranz and Scholz [1977], all samples were deformed in the same hydraulic servo-controlled apparatus. The axial load, applied through a piston to the ends of the sample, can be preset to reach and maintain a specified value (within 1 bar) at a specified loading rate. In addition, a hydrostatic confining pressure can be applied and maintained constant independently of the axial load. Kerosene was used for the confining medium. The loading procedure for each sample, again excepting the uniaxial tests, was the same. First, a hydrostatic pressure of 100, 250, 530, 1000 or 2000 bars was applied to the sample. Next a few additional bars were applied to the ends of the sample to seat the piston against it.

A load was selected and applied at 100 bars sec^{-1}. For a fracture test, the load was set high enough to achieve fracture. For a creep test, the load was set at a value of from 95% to 75% of the stress achieved during the fracture test at the corresponding pressure. At each pressure, at least one test was made at 87% of the stress difference achieved during the fracture test.

Several tests at 530 bars and 1000 bars of pressure at 87% of the corresponding fracture strengths were stopped at, or shortly after, the onset of tertiary creep. The sample was unloaded and internal sections of the sample removed for examination with the scanning electron microscope (SEM). These tests were made to augment others by the author [Kranz, 1979a] on samples fatigue tested under atmospheric pressure. The same sample preparation and crack-counting techniques were used.

The strains ε_r, ε_z and $\Delta V/V$ were recorded continuously on strip chart recorders. Both ε_r and ε_z from the 2.54 cm gauges were recorded against the output from an external load cell. Individual values of strain are accurate to $\pm 10^{-4}$. Load cell output was accurate to 2%. No effort was made to increase the load to offset increases in cross-sectional area of the sample which may have reached 2%. Thus actual values of stress difference reported are accurate only to within 4%. Confining pressure, measured with both a Heise gauge and a BLH pressure transducer, was maintained constant and known accurately to within 1%.

Times to failure and times to the onset of tertiary creep (where strain rate starts increasing) were recorded. In practice, picking

the onset of tertiary creep is a matter of laying a straight-edge against each of the strain vs. time records and deciding where the slope changes from concave downward to concave upward. Usually the radial strain (ε_r) curves show this inflection point before either the longitudinal strain ε_z or volumetric strain curves. Tertiary creep onset time reported here is the time after loading has ceased to the earliest inflection point on any of the strain curves. The accuracy of this time and the failure time depends on the length of the experiment because recorder speed was chosen on this basis. Uncertainty is estimated at 0.1%.

OBSERVATIONS AND ANALYSIS

Table 1 and Table 2 present the data from the fracture and creep tests, respectively. Notes at the bottom of each table explain the column headings. Fracture strength as a function of confining pressure is shown in Figure 1. Figure 2 shows the logarithm of creep rupture time in seconds as a function of the applied stress difference in kilobars at four different pressures.

Rupture times and theories of static fatigue

Based upon their experimental work on quartz [Martin, 1972; Scholz, 1972] Scholz and Martin proposed that the static fatigue of rock could be described by

$$t_f = t_o P_{H_2O}^{-\alpha} \exp\left(\frac{E}{RT} - k\sigma\right) \qquad (1)$$

where t_f is the time to failure in seconds, P_{H_2O} is the partial pressure of water presumably in the cracks, σ is the applied stress in kilobars and t_o, α, E and k are constants. Equation (1) is based on data taken at atmospheric pressure and there is no reason to believe the constants are independent of pressure or that one can substitute stress difference for the σ term. The data presented in Table 2 provide a valid test of equation (1), even though the initial P_{H_2O} was not very well controlled; the sample was prepared under ambient laboratory conditions.

Equation (1) can be rewritten in the form

$$\log (t_f) = A + B\sigma \qquad (2)$$

where $A = \ln [t_o P_{H_2O}^{-\alpha}] + E/2.303\ RT$ and

$B = -k/2.303$. Table 3 lists the values of A and B derived by fitting equation (2) to the data of Table 2 and also Wawersik's [1972] data for water-saturated Westerly granite (WG). Uncertainties for the slopes, B, are the standard deviations on the fit. Within these limits k doesn't change very much. There is a strong pressure dependence in the A term, however, and this may be due to either a decrease in P_{H_2O} or increase in activation energy. Significantly, the completely saturated granite has the lowest A value.

Subjected to a hydrostatic confining pressure cracks close, squeezing out some of the air and moisture within the rock. When deviatoric stresses cause dilatancy, P_{H_2O} decreases within the cavity spaces which open. As there is a small increase in the amount of dilatancy at the onset of tertiary creep with increasing pressure (Δ_2 in Table 2), it is quite likely that part of the pressure dependence in the A term of equation 2 is a result of lower P_{H_2O} values. Equally possible is an increase in the activation energy term in (1) with pressure. Scholz and Martin neglected to include a pressure term in their formulation because their tests were all performed at the same pressure. In (1), E should be replaced by E* + PV* where E* is the activation energy for the rate governing process, P is pressure and V* is the activation volume.

Cruden [1974] derived a static fatigue law different in form from equation 2. He started by postulating that the strain at the onset of tertiary creep is constant. We defer a discussion of this postulate until the next section. Further, he assumed that the time to the onset of tertiary creep is proportional to the time to fracture. Analysis of the data in Table 2 shows this hypothesis cannot be rejected at the 95% confidence level. Thus we assume

$$a_1 T = t_f \tag{3}$$

and using a power law dependence of strain on time and stress,

$$\varepsilon(T,\sigma) = a_2 = \varepsilon_o + a_3 \sigma^N T^m$$

Combining this with (3) leads to

$$t_f = a_4 \, \sigma^{-N/m} \tag{4}$$

or

$$\log t_f = A' + B' \log \sigma \tag{5}$$

with $A' = \frac{1}{m} \log \left[\frac{a_1^{\,m} (a_2 - \varepsilon_o)}{a_3} \right]$ and $B' = \frac{-N}{m}$

In his model [Cruden, 1970] N and m can be related to the stress corrosion rate and microcrack population. Equation 5 was fit to the data in Table 2. The values for A' and B' are given in Table 3 assuming that $\sigma = \sigma_1 - \sigma_3$.

Does equation 2 or equation 5 fit the data better? Two estimates of goodness of fit have been calculated. The first is simply the mean square residual (MSR) between the predicted value of log t_f and the real value of log t_f. The smaller this value is, the "tighter" the fit. The second estimator, R^2, is a measure of how close the model comes to fitting the data exactly. If the model were the "correct" one, R^2 would be unity. R^2 is the square of the multiple correlation coefficient [Draper and Smith, 1966; page 62] and can be used as a measure of the adequacy of the model to fit the data.

Table 3 indicates that both equation 2 and equation 5 can be made to fit the data adequately. (A computer program employing double

precision was used.) They are equally "correct" statistically at any particular pressure. When all the data (excepting that for WG) are used, however, assuming $\sigma = \sigma_1 - \sigma_3$, both equations 2 and 5 are very poor because of the additional pressure dependence in the coefficients.

The similarity of the forms and the fact that stress corrosion of cracks is the foundation of both theories, leads one to inquire if another, more general, model could be as adequate for predictive purposes. Several models were chosen. The best one had the form

$$\log t_f = a'' + B''\sigma_1^{P} + C''\sigma_3^{S} \qquad (6)$$

This model reduces to equation 2 if $\sigma_3 << \sigma_1$ and P is near unity. Table 3 indicates that equation 6 is much better than equations 2 or 5 at fitting all the data but it still has room for improvement ($R^2 = .81$). Note that P has a value close to one so it is easy to see a direct correspondence between the functional forms of the coefficients in equations 6 and 2.

Inelastic strain

It is now well established that creep in brittle rocks is a consequence of microcracking [Scholz, 1968; Cruden, 1970; Wu and Thomsen, 1975], even under pressure [Lockner and Byerlee, 1977]. Since cracking is an inelastic process, attention should be focused on the inelastic part of the recorded strain. Kranz and Scholz [1977] sug-

gested that the inelastic volumetric strain is a measure of the crack density within the rock.

Tables 1 and 2 list the inelastic strain components ε^*_z and ε^*_r as well as the inelastic volumetric strains Δ. Figure 3 shows the inelastic volumetric strains at each pressure and stress difference. For the fracture tests, Δ was recorded near the failure stress, just prior to the point where the fidelity of the strain gauge readings became questionable; that is, near the point in stress-strain space where the instability leading to failure occurred. These points are plotted as open symbols in Figure 3 at the σ/σ_c value where they were measured. The solid symbols are the Δ_2 values calculated or measured at the onset of tertiary creep in each creep experiment.

Kranz and Scholz [1977] claim that if a critical crack density is to be associated with an unstable condition within the rock, the inelastic volumetric strain at the onset of the instability should be roughly constant, independent of the applied stress. In Table 4 this hypothesis is evaluated at each pressure. The standard deviation of Δ at each pressure is less than 10% of the average except for the uniaxial data. The correlation coefficient between σ/σ_c and Δ is small, and a T test shows that the hypothesis of a linear correlation between σ/σ_c and Δ can be rejected at each pressure. Thus it seems that the instability can be marked by a critical dilatant volume, but the magnitude of this inelastic volume is a function of pressure, at least up to 2 Kb.

A comparison of the inelastic volumetric strain near the instability in the fracture tests with that at the onset of tertiary creep

is made in Figure 4 as a function of pressure. The value of Δ in the constant-rate fracture tests depends, of course, on the stress level chosen to mark the instability. Even taking this into consideration there is a rise with pressure in the dilatant volume which the rock can stably sustain. Brace [1978, Table 2] and Brace et al. [1966, Table 3] show a similar result for other rocks, and Wawersik and Brown [1973] also found the maximum allowable strain increases as confining pressure is raised. Analogously, there is an increase in Δ with pressure at the onset of tertiary creep. The dilatant volume at the instability is the same within a factor of two in the two different tests. Even considering the uncertainty in determining this instability with strain gauges, it suggests that a similar critical crack density, or some other crack ensemble parameter, must be achieved in both test types before the crack ensemble becomes unstable. Whatever happens to the crack ensemble in the last 2-5% of a constant-rate test probably also occurs in the tertiary phase of static fatigue.

The process of accumulating crack volume is initially slower in a creep test, and apparently allows more strain to build up than in the fracture test. Wawersik and Brown [1973] and Scholz and Koczynski [1979] have also reported larger accumulated strains in creep tests than in faster, constant loading rate tests. In the next section we give observational evidence that the increase in dilatant volume sustained with pressure is related to size and number of cracks.

SEM Observations of Cracks

By stopping uniaxial creep experiments at various times and then sectioning the sample, Kranz [1979a] was able to study the trend of

crack growth as a function of time using the scanning electron microscope (SEM). Average stress-induced crack lengths increased with time as much or more than they did upon loading. In addition, crack interaction with other cavities seemed to increase with time. It was suggested that near the onset of tertiary creep crack coalescence was more important than individual crack growth in determining rock stability. Almost all stress-induced cracks were extensional.

In this study, the stress-induced crack length and angle spectra were compiled at the onset of tertiary creep for samples subjected to the same σ/σ_c value (87%) as the uniaxial samples, but at confining pressures of 530 and 1000 bars. Analysis was done on block A samples only. The data are compared in Figure 5 and tabulated in Table 5. Note, in Table 5, that though only half as many traverses across the sample area were made on the two samples subjected to pressure, at least 30% more cracks were counted. In addition, the average crack length in the latter was greater, though crack length was extremely variable. The number of cracks with lengths greater than 500 μm was greater in the samples subjected to pressure. Average width was only slightly greater and also quite variable. The average angle to the maximum stress direction and the spread of crack angles was the same.

Figure 5 makes these points more clearly. One hundred representative cracks are presented. Each unit is one crack counted within the appropriate 50 μm × 10° slot. The histograms are quite similar. Most short cracks are within 30° to the maximum stress axis

and the longest cracks are within 10°. Those cracks at angles greater than 30° are invariably short. At the higher pressures, there are more of these. This roughly corresponds to the slight increase in the ultimate fracture angle as pressure increases (Table 2). Many of these short, off-angle cracks were linking cracks, joining longer ones. The histrograms show that at the onset of tertiary creep, the crack ensemble has a definitive character and, with the exceptions noted, it is the same near the onset of the instability independent of pressure.

Creep equations

Time-dependent deformation, whether in metals, ceramics or rocks, has been described using one of three different equation forms: logarithmic, inverse exponential or a power function with exponent less than unity. Often a steady-state factor, proportional to time under load, is added on. At least within the rock mechanics literature, there is no consensus as to which is the best for predictive purposes. Each has its own phenomenological derivation and historical precedent [see reviews by Misra and Murrell, 1965 and Cruden, 1971]. It therefore seemed prudent to try all of them. This is essentially the same approach taken by Arfrouz and Harvey [1974]. They concluded that equations with time appearing to a power gave the best fit to the data for rocks such as coal, limestone and sandstone. Cruden [1971] reached the same conclusion. He also concluded that the steady-state term was insignificant.

All of the above curve-fitting exercises were conducted on uniaxial longitudinal strain data. As it seemed possible that strain perpendicular to the applied load might not follow the same equation, or that the equations might change with pressure, all the strain data, at all pressures were fit using least-squares regression techniques. Strain was fit as a function of time starting one second after the loading and up to the onset of tertiary creep. The results may be stated as follows [Kranz, 1979b]:

1. At all pressures, either

$$\varepsilon(t) = A + B\log t + Ct \tag{7}$$

or

$$\varepsilon(t) = A + Bt^{m} + Ct \tag{8}$$

could be made to fit the data to a degree much better than the accuracy of the data.

2. Using several criteria for goodness of fit, equation 7 fit "best" about 50% of the time for the ε_z component but only 25% of the time for either ε_r or $\Delta V/V$ for the uniaxial experiments. The remainder of the data was best fit by equation 8 with or without a Ct term.
3. Equation 8 without the Ct term almost invariably gave the "best fit" at higher pressures for <u>all</u> strains. and when it didn't, including the Ct term made it the best.

4. In all cases where a term proportional to time was necessary, the proportionality constant was of the order of 10^{-6} or less when time is given in seconds.
5. The coefficients A, B and C were strongly stress-dependent. The stress or pressure dependence of m in (8) remains unclear.

Since equation 8 was most successful an attempt was made to find the σ_1 and σ_3 dependence of the coefficient B. Transient creep at higher temperatures [Carter and Kirby, 1978] has most often been written in the form

$$\varepsilon = \beta_o \sigma^N t^m \exp(-E/RT) \tag{9}$$

Therefore, all the data were refit, using an iterative technique [Kranz, 1979b], to the form

$$\varepsilon(t, \sigma_1, \sigma_3) = \alpha + \beta(\sigma_1 - \sigma_3)^N t^m \tag{10}$$

The results for equation 8 are given in Table 6. Equation 10, given in Table 7, is only a fair model and there still may be a pressure dependence within the coefficients. It suggests that

$$\varepsilon(t, \sigma_1, \sigma_3) = \alpha + \beta(\sigma_1^{N_1} - \sigma_3^{N_3})t^m \tag{11}$$

might be better. Equation 11 has the additional virtue of providing a quick estimate of the relative effects of σ_1 and σ_3 on the creep rate. To determine the best values of α, β, N_1, N_3 and m simultaneously requires 5 pieces of information, or 4 at every time t. As σ_1 and σ_3 were not changed during an experiment, equation 11 cannot be uniquely defined from this data set. An experiment where σ_3 is incrementally changed, for example, is needed to find the relative values of N_1 and N_3. If we accept the m value for each experiment as defined by equation 8, however, then it is possible to fit B in equation 8 to the form

$$B = \beta(\sigma_1^{N_1} - \sigma_3^{N_3}) \tag{12}$$

using all the data with m as an additional input. We find $N_1 = 4.2$, $N_3 = 5$ with $\beta = -1.1 \times 10^{-6}$ for ε_z and $N_1 = .5$, $N_3 = 1.5$ with $\beta = 4.15 \times 10^{-3}$ for ε_r. The fits are poor ($R^2 \simeq .4$), however, probably because of the large covariance of N_1, N_3 and m. As a result, little meaning can be attached to these values, other than to say that the strain rate, being proportional to B, is affected more by σ_3 than by σ_1.

DISCUSSION

The effect of pressure

As this and many other studies have shown, confining pressure increases the differential stress which a rock can sustain before fracturing. If a stress difference less than the fracture stress is applied, confining pressure increases the fatigue time. If we take into account the increase in strength with pressure, is this sufficient to allow us to predict the static fatigue time? That is, if we normalize the applied load to the short-term breaking strength at the corresponding pressure, will the data lie on a common fatigue curve?

Figure 6 shows the log of the failure time as a function of the applied stress difference normalized to the maximum stress difference sustained in the fracture tests at the corresponding pressure. The best-fit lines from Figure 2 have been redrawn on this new stress axis. Some of the lines intersect at high stress as a result of data scatter and different amounts of time to complete loading. The slopes, however, indicate that the pressure effect increases with increasing pressure. For example, at an applied load of 87% of the fracture stress (symbols), the time to failure increases with pressure. Note also that the water-saturated granite (WG) is more susceptible to stress than the nominally dry granite.

It might be argued that since microcracking and crack coalescence are the basic mechanisms of brittle failure in both the short-term

strength test and the creep test, then the pressure effect on crack growth and coalescence should be the same in both tests. This may not be so. Pressure does not affect the nucleation of microcracks but it does increase the energy barrier to be overcome for continued propagation [Francois and Wilshaw, 1968]. The difference between the creep test and rapid fracture test lies in the method of overcoming the energy barrier. In the fracture test, the energy is supplied by the continuously augmented deviatoric stress. The cracks are, in a sense, driven to greater lengths and interaction. At constant stress difference (creep test) cracks propagate into a stable position and stop [Brace and Bombolakis, 1963; Martin, 1972], and further growth occurs when the energy barrier is lowered by stress corrosion reactions at the crack tip [Hillig and Charles, 1965]. Thus in the fracture test, crack growth and coalescence are limited primarily by the stress rate while in the creep test they are limited by the corrosion reaction rate or by the rate at which corrosive agents can get to the crack tips [Martin, 1972].

In order to understand the effect of pressure on static fatigue as indicated by Figure 6, microcracking is considered to be a thermally activated process. Lindholm et al. [1974] show that fracture is controlled by such a process. As such, it occurs at a rate proportional to $\exp(-\Delta H/RT)f(\sigma)$ where ΔH is the activation enthalpy associated with the energy barrier at the crack tip, and $f(\sigma)$, a function of the applied stress, is usually given as $\exp(K\sigma)$ or σ^N. $\Delta H = E^* + PV^*$ where E^* is the activation energy, V^* is the activation volume and P is pressure. Thus pressure acts to decrease the rate at which work is done at the crack tip.

One way pressure could affect static fatigue is through its effect on the stress corrosion process. Stress corrosion is a thermally activated process [Hillig and Charles, 1965] which occurs at a rate proportional to

$$\exp\left[-\left(\frac{\Delta H' - \Delta H}{RT}\right)\right]$$

where, to first order, $\Delta H' = E^* - (\sigma_1 - \sigma_3)V^*$ and $\Delta H = E_o - \gamma V_{m/\rho}$ where γ is the crack surface free energy, V_m is the molar volume and ρ is the crack tip radius. Thus deviatoric stress increases the corrosion rate while any factor which decreases ρ or increases γ will decelerate the corrosion process. The effect of pressure on the corrosion rate is not specifically accounted for in this formulation and must come through its effect on ΔH (by changing ρ for example) or by some additional PV^* term in $\Delta H'$. Dehart and Liebowitz [1968] have shown, for example, that stress corrosion is retarded by pressure in some metals, but little other evidence is available.

Besides increasing the crack propagation energy required and the fracture toughness [Schmidt and Huddle, 1977], pressure increases the mean normal stress on any plane within the rock. This would be important if friction were a factor in crack growth. The vast majority of stress-induced cracks in both constant rate and creep tests are extensional, not shear cracks, however [Tapponnier and Brace, 1976; Kranz, 1979a], so the increased normal stress is probably more of a factor in closing crack walls. If a crack closes under pressure, the transport of fluids and gases through the rock is reduced and this will have an

incidental effect on the corrosion process during creep if new crack surfaces cannot be reached by corrosive agents.

In a creep test, the rate of individual crack growth which is controlled by the rate of stress-corrosion, will determine to a large extent, the fatigue time. The rate of crack-linking will also affect the fatigue time and it is not clear that pressure will have the same effect on the crack-linking process as on the individual crack growth process. Figure 4 shows that the higher the pressure, the larger the crack volume prior to the failure instability. This seems to indicate that pressure severely inhibits the crack-linking process. As this occurs in both rapid constant-rate tests and creep tests, the rate limiting factor for crack-linking cannot be the same as for individual crack growth. Apparently, stress-corrosion cracking in the creep test or stress-induced cracking in the constant-rate test are initially dominant and the crack coalescence rate is only significant near the end of an experiment when the critical crack density is approached. The mechanism by which pressure inhibits crack linking is unknown but may involve a diminishing of the stress concentration around each crack as a result of the superposition of the least principal stress, or a decrease in the shear stress for the same reason.

Static fatigue in the upper crust

To relate the results of this study to the production of faults or fractures within the Earth, one must be willing to accept a large

extrapolation in time. If we assume that fatigue rupture can only occur at stresses above the dilatancy point (C' in Table 1, where the values are biased toward the low side) then, using equation 6, we can estimate the fatigue time at depth.

Figure 7 shows the amount of time that dry granite could sustain a particular stress state. Qualitatively, the chemical effects of pore water and temperature would shift the curves downward. Even conceding several orders of magnitude to these effects, it is obvious that for creep rupture of whole rock to occur in the upper crust, large deviatoric stresses are necessary. For example, assuming completely saturated granite so that the σ_3 depth gradient is 166 bars/km, at 3 km depth a stress difference of 2.5 kilobars could be sustained for over 31 million years (10^{15} sec). At this depth, the temperature is less than 100°C but its effect on the stress corrosion process could be considerable. Using an activation energy of 1.4 kcal/mole for granite [Carter and Kirby, 1978; Table 1] the time to fracture at 90°C is about 2 orders of magnitude less than that at 24°C under otherwise identical conditions.

CONCLUSIONS

To summarize, the results of this study indicate that the effect of pressure is to decrease creep rates, increase fatigue failure time and increase the amount of inelastic deformation rock can sustain before becoming unstable. The pressure effect can be traced primarily

to an increase in the activation enthalpy required for the stress corrosion process governing the creep rate. Ancillary pressure effects possibly include the decrease in P_{H_2O} as dilatancy grows with time and the decrease in crack interaction. The total pressure effect on static fatigue is more severe than would be expected from a consideration of the pressure effect on fracture strength alone.

Experiments with conditions closer to those found in the crust are needed. In particular, the individual effects of pore pressure and temperature under crustal stress regimes need much further study in order to characterize the brittle-ductile transition zone. This study has shown that large differential stresses can be sustained in whole rock at shallow depths for long periods of time but this may not be the case at greater depths.

Acknowledgments. Conversations with Terry Engelder, David Holcomb, and Chris Scholz helped clarify a number of points. Reviews of the manuscript by Scholz, Engelder, and Paul Richards are greatly appreciated. This work was supported by National Aeronautics and Space Administration grant NGR 33-008-146 and by National Science Foundation, Division of Earth Sciences, grant EAR 77-22689. Lamont-Doherty Geological Observation Contribution No. 0000.

REFERENCES

Arfouz, A., and J. M. Harvey, Rheology of rocks within the soft to medium strength range, *Int. J. Rock Mech. Min. Sci., 11,* 281-290, 1974.

Brace, W. F., Volume changes during fracture and frictional sliding: a review, *Pure Appl. Geophys., 116,* 603-614, 1978.

Brace, W. F., and E. G. Bombolakis, A note on brittle crack growth in compression. *J. Geophys. Res., 68,* 3709-3713, 1963.

Brace, W. F., B. Paulding, and C. Scholz, Dilatancy in the fracture of crystalline rocks, *J. Geophys. Res., 71,* 3939-3953, 1966.

Carter, N. L., and S. H. Kirby, Transient creep and semi-brittle behavior of crystalline rock, *Pure Appl. Geophys., 116,* 807-839, 1978.

Cogan, J., Triaxial creep tests of Ophonga limestone and Ophis shale, *Int. J. Rock Mech. Min. Sci., 13,* 1-10, 1976.

Cruden, D. M., A theory of brittle creep in rock under uniaxial compression, *J. Geophys. Res., 75,* 3431-3442, 1970.

Cruden, D. M., The form of the creep law for rock under uniaxial compression, *Int. J. Rock Mech. Min. Sci., 8,* 105-126, 1971.

Cruden, D. M., The static fatigue of brittle rock under uniaxial compression, *Int. J. Rock Mech. Min. Sci., 11,* 67-73, 1974.

Dehart, R. C., and H. Liebowitz, The influence of ambient pressure on the stress corrosion susceptibility of metals, *Eng. Fract. Mech., 1,* 129-135, 1968.

Draper, N. R., and H. Smith, *Applied Regression Analysis*, 407 pp., John Wiley and Sons, New York, 1966.

Francois, D., and T. R. Wilshaw, The effect of hydrostatic pressure on the cleavage fracture of polycrystalline materials, *J. Appl. Physics, 39*, 4170-4177, 1968.

Griggs, D., Deformation of rocks under high confining pressures, *J. Geol., 44*, 541-577, 1936.

Griggs, D., Creep of rocks, *J. Geol., 47*, 225-251, 1939.

Hadley, K., Dilatancy in rock at elevated temperatures (Abstract), *Trans. Amer. Geophys. Union, 56*, 1060, 1975a.

Hadley, K., Azimuthal variation of dilatancy, *J. Geophys. Res., 80*, 4845-4850, 1975b.

Heard, H. C., Comparison of the flow properties of rocks at crustal conditions, *Phil. Trans. Roy. Soc. London, A-283*, 173-186, 1976.

Hillig, W. B., and R. J. Charles, Surfaces, stress-dependent surface reactions and strength, in *High Strength Materials*, edited by V. Zackay, pp. 682-705, John Wiley and Sons, New York, 1965.

Jaeger, J. C., and N. G. W. Cook, *Fundamentals of Rock Mechanics*, 2nd edit., Halsted Press, New York, 1976.

Kranz, R. L., Crack growth and development during creep of Barre granite, *Int. J. Rock Mech. Min. Sci.*, in press, 1979a.

Kranz, R. L., The static fatigue and hydraulic properties of Barre granite, Ph.D. thesis, Columbia University, New York, 1979b.

Kranz, R. L., and C. H. Scholz, Critical dilatant volume of rocks at the onset of tertiary creep, *J. Geophys. Res., 82*, 4893-4898, 1977.

Lockner, D., and J. Byerlee, Acoustic emission and creep in rock at high confining pressure and differential stress, *Bull. Seismol. Soc. Amer., 67,* 247-258, 1977.

Martin, R. J., Time-dependent crack growth in quartz and its application to the creep of rocks. *J. Geophys. Res., 77,* 1406-1419, 1972.

Misra, A. K., and S. A. F. Murrell, An experimental study of the effect of temperature and stress on the creep of rocks, *Geophys. J. Roy. Astron. Soc., 9,* 509-535, 1965.

Robertson, E. C., Creep of Solenhofen limestone under moderate hydrostatic pressure, *Geol. Soc. Amer. Mem. 79,* 227-244, 1960.

Schmidt, R. A., and C. W. Huddle, Effect of confining pressure on fracture toughness of Indiana limestone, *Int. J. Rock Mech. Min. Sci., 14,* 289-291, 1977.

Scholz, C. H., Mechanism of creep in brittle rock, *J. Geophys. Res., 73,* 3295-3302, 1968.

Scholz, C. H., Static fatigue of quartz, *J. Geophys. Res., 77,* 2104-2114, 1972.

Scholz, C. H., and T. A. Koczynski, Dilatancy anisotropy and the response of rock to large cyclic loads, *J. Geophys. Res.,* in press, 1979.

Tapponnier, P., and W. F. Brace, Development of stress-induced microcracks in Westerly granite, *Int. J. Rock Mech. Min. Sci., 13,* 103-112, 1976.

Tullis, J., and R. A. Yund, Experimental deformation of dry Westerly granite, *J. Geophys. Res., 82,* 5705-5718, 1977.

Wawersik, W. R., Time-dependent rock behavior in uniaxial compression,

Proc. 14th Symp. Rock Mech., pp. 85-106, Penn. State Univ., University Park, Pa., 1972.

Wawersik, W. R., and W. S. Brown, Creep fracture of rock, Tech. Rep. *UTEC ME 73-197*, pp. 1-40, Eng. Dept., University of Utah, Salt Lake City, 1973.

Williams, F. T., and M. A. Elizzi, An apparatus for the determination of time dependent behavior of rock under triaxial loading, *Int. J. Rock Mech. Min. Sci., 13*, 245-248, 1976.

Wu, F. T., and L. Thomsen, Microfracturing and deformation of Westerly granite under creep conditions, *Int. J. Rock Mech. Min. Sci., 12*, 167-173, 1975.

TABLE 1. Data from Fracture Tests

Sample	σ_c (Kb)	P_c (Kb)	c' (Kb)	σ' (%)	ε^*_z ($\times 10^{-3}$)	ε^*_r ($\times 10^{-3}$)	Δ	Fracture Angle (± 5°)
1	2.2	.001		95	-3.3	2.0	0.7	
2	2.29	.001		95	-3.5	2.0	0.5	
45A	2.92	.1	.9	96	-2.5	2.6	2.7	20
43A	3.65	.25	1.75	97	-3.4	4.5	5.6	15
4A	4.7	.5	1.7	97	-4.4	5.6	6.8	
17A	4.8	.53	1.5	97	-5.2	5.8	6.4	25
1A	6.25	1.0	2.6	97	-6.1	7.0	7.9	25
22B	6.27	1.0	2.75	97	-5.2	6.3	7.4	35
23B	6.4	1.0	2.6	97	-6.2	6.9	7.6	25
31B	8.4	1.98	3.0	98	-6.0	6.9	7.8	30
32B	8.7	2.0	2.8	98	-6.7	7.3	7.9	35
2A	9.38	2.5	3.0	99	-6.7	7.8	8.9	30
3A	12.9	4.2	3.8	99	-8.8	11.2	13.6	

σ_c is the maximum stress difference achieved = $\sigma_1 - \sigma_3$
P_c is the confining pressure = σ_3
c' is the dilatancy point as defined by *Brace et al.* [1966]
σ' is the % of σ_c at which strains were recorded
ε^*_z, ε^*_r are the inelastic longitudinal and radial strains from 2.54 cm gauges except for samples 1 and 2 where strains are from 1.27 cm gauges.
Δ is the inelastic volumetric strain = $2\varepsilon^*_r + \varepsilon^*_z$

TABLE 2. Data from Creep Tests

Sample	σ/σ_c	σ (Kb)	P_c (Kb)	t_f (sec)	T (sec)	ε_z	ε_r	ε^*_z	ε^*_r	Δ_1	Δ_2	Frac. Angle (± 5°)
						($\times 10^{-3}$)						
15	0.74	1.62	.001	1.6×10^6	1.46×10^6	-3.60	2.11	-0.9	1.29		1.68	
14	0.79	1.73	.001	2.3×10^2	8.0×10^1	-3.40	2.0	-0.5	1.11		1.73	
12	0.80	1.77	.001	2.29×10^4	1.65×10^4	-3.31	1.65	-0.36	0.77		1.18	
13	0.81	1.79	.001	1.14×10^3	4.92×10^2	-3.74	2.08	-0.75	0.99		1.23	
4	0.84	1.85	.001	650	265	-4.22	1.87	-1.14	0.95		0.76	
3	0.85	1.88	.001	505	235	-4.13	2.21	-1.0	1.26		1.52	
10	0.89	1.96	.001	435	210	-4.16	1.81	-0.9	0.84		0.78	
11	0.90	1.99	.001	149	62	-4.95	2.64	-1.64	1.55		1.46	
20	0.92	2.03	.001	11.5	4.5	-6.28	3.01	-2.7	1.75		0.80	
46A	0.87	2.52	.1	562	305	-6.5	5.04	-1.8	3.1		4.4	20
44A	0.87	3.18	.25	1.05×10^4	8.15×10^3	-7.0	6.16	-2.3	4.15		6.0	25
7A	0.81	3.95	.53	3.55×10^5	3.37×10^5	-12.86	10.08	-4.29	7.3	10.31	8.35	25
9A	0.84	4.10	.53	1.59×10^5	1.12×10^5	-11.55	9.8	-3.78	6.9	10.02	6.67	25
10A	0.85	4.13	.53	1.22×10^5	1.03×10^5	-10.64	8.9	-3.52	6.6	9.68	6.28	15
12A	0.87	4.22	.55	1.29×10^4	1.17×10^4	-12.0	9.3	-4.5	6.5	8.5	7.7	25
13A	0.89	4.31	.55	2.95×10^4	2.45×10^4	-13.0	8.95	-4.05	6.25	8.45	7.07	15
14A	0.91	4.4	.53	3.03×10^3	2.22×10^3	-12.3	9.3	-4.45	6.9	9.35	8.33	20
15A	0.93	4.5	.54	525	390	-11.65	8.82	-4.0	6.2	8.4	7.81	15
16A	0.95	4.6	.53	252	145	-14.12	11.0	-6.25	8.5	10.75	.95	10

TABLE 2. Data from Creep Tests (continued)

Sample	σ/σ_c	σ (Kb)	P_c (Kb)	t_f (sec)	T (sec)	ε_z	ε_r	ε^*_z	ε^*_r	Δ_1	Δ_2	Frac. Angle (± 5°)
						($\times 10^{-3}$)						
18A	0.86	5.4	1.0	7.14×10^5	6.82×10^5	-12.8	10.3	-3.5	7.6	11.7	10.4	
27B	0.87	5.5	1.01	1.19×10^5	9.72×10^5	-12.6	8.8	-3.9	6.5	9.1		25
26B	0.88	5.55	1.01	1.84×10^4	1.41×10^4	-14.0	9.6	-5.2	7.2	9.2	9.2	30
29B	0.91	5.75	1.02	2.54×10^3	1.98×10^3	-14.6	11.8	-5.9	8.8	11.7	9.6	25
30B	0.93	5.9	1.0	1.09×10^3	7.26×10^2	-15.6	11.4	-5.8	7.4	9.0		25
34B	0.87	7.6	1.98	9.3×10^5	7.8×10^5	-18.6	12.0	-6.6	8.5	10.4	10.3	35
36B	0.89	7.75	1.98	1.75×10^4	$1.[illegible] \times 10^4$	-22.0	12.8	-8.6	9.8	11.0	9.6	30
35B	0.91	7.9	1.98	3.65×10^3	2.68×10^3	-22.1	12.1	-8.8	9.8	10.8	9.9	30

σ is the applied stress difference = $\sigma_1 - P_c$
σ/σ_c is the stress difference normalized to the stress difference at failure in a fracture test at the corresponding confining pressure
t_f is the time to failure
T is the time to the onset of tertiary creep
ε_z, ε_r are total strains achieved at time T (from 2.54 cm gauges)
ε^*_z, ε^*_r are the inelastic strains achieved at time T (from 2.54 cm gauges)
$\Delta_1 = 2\varepsilon^*_r + \varepsilon^*_z$ at time T
Δ_2 = inelastic volumetric strain at time T from 1.27 cm gauge configuration connected on sample or from calculated principal strains
all strain $\times 10^{-3}$

TABLE 3. Parameters for Static Fatigue Equations

P_c (Kb)	.001 (WG)	.001	.53	1.0	2.0	All Data
Equation 2						
A	14.8	23.2	26.4	35.4	66.6	2.9
B	-5.0 ± 2.6	-10.8 ± 2.8	-5.2 ± 2.8	-5.5 ± 1.1	-8.0 ± 1	-.23 ± .01
MSR	.012	.226	.07	.083	.062	1.6
R^2	.96	.89	.941	.922	.939	.12
Equation 5						
A'	11.3	15.4	36.3	58.5	132	2.7
B'	-21.9 ± 11.7	-45.8 ± 11.8	-51 ± 17	-72 ± 31	-143 ± 84	-2.05 ± .79
MSR	.014	.205	.077	.078	.058	1.47
R^2	.95	.90	.936	.929	.94	.12
Equation 6						
A"						17.2
B"						-8.22 ± 2.4
C"						31.8 ± 3.4
P						.9
S						.7
MSR						.314
R^2						.812

TABLE 4. Evaluation of Inelastic Volumetric Strain Data

P_c (Kb)	Number of Points	Average Δ	Standard Deviation	Correlation Coefficient
		($\times 10^{-3}$)		
.001	9	1.24	.37	-.5942
.53	8	7.4	.72	.02715
1.0	5	9.46	.51	-.5090
2.0	3	9.93	.29	-.5694

TABLE 5. SEM Data

Confining Pressure (bars)	1	530	1000
Stress level: σ/σ_c	87%	87%	87%
Number of cracks*	172	246	254
Average length (μm)	172	230	245
± Standard deviation	± 181	± 282	± 302
Average width (μm)	0.17	0.20	0.19
± Standard deviation	± 0.07	± 0.10	± 0.08
Average angle	16	13	16
± Standard deviation	± 27	± 25	± 28
Cracks > 500 μm length	14	34	32
Cracks > 30° to σ_1	19	24	34

*20 traverses across the sample were made for the 1 bar samples whereas only 10 traverses were made across the same area in the other two samples.

TABLE 6a. $\epsilon_z = A + Bt^m$

Sample	σ (Kb)	P_c (Kb)	A	B	m	MSR	R^2
46A	2.52	.1	-5.3×10^{-3}	-8.77×10^{-3}	.01	2.9×10^{-10}	.99
44A	3.18	.25	-1.94×10^{-3}	-3.37×10^{-3}	.04	2.7×10^{-9}	.98
7A	3.95	.53	-6.24×10^{-3}	-3.04×10^{-3}	.06	5.7×10^{-9}	.99
9A	4.1	.53	-8.02×10^{-3}	-1.87×10^{-3}	.06	1.5×10^{-8}	.94
10A	4.13	.53	-7.81×10^{-3}	-7.44×10^{-4}	.1	2.7×10^{-9}	.99
12A	4.22	.55	-7.69×10^{-3}	-1.31×10^{-4}	.1	4.8×10^{-8}	.94
13A	4.31	.55	-9.19×10^{-3}	-1.03×10^{-3}	.12	6.3×10^{-9}	.98
14A	4.4	.53	-9.18×10^{-3}	-7.04×10^{-4}	.19	2.5×10^{-9}	.99
15A	4.5	.54	-1.0×10^{-2}	-1.7×10^{-4}	.42	5.9×10^{-9}	.98
16A	4.6	.53	-5.3×10^{-3}	-5.03×10^{-3}	.1	4.2×10^{-8}	.95
18A	5.4	1.0	-1.03×10^{-2}	-4.70×10^{-5}	.27	6.3×10^{-9}	.98
27B	5.5	1.01	-1.02×10^{-2}	-2.39×10^{-4}	.2	5.9×10^{-9}	.98
26B	5.55	1.01	-1.08×10^{-2}	-9.47×10^{-4}	.13	5.0×10^{-9}	.98
29B	5.75	1.02	-1.0×10^{-2}	-1.80×10^{-3}	.1	6.7×10^{-9}	.88
30B	5.9	1.0	-1.13×10^{-2}	-6.29×10^{-4}	.2	3.1×10^{-9}	.98
34B	7.6	1.98	-1.64×10^{-2}	-1.07×10^{-4}	.28	2.0×10^{-9}	.98
36B	7.75	1.98	-1.55×10^{-2}	-2.57×10^{-3}	.1	1.6×10^{-7}	.89
35B	7.9	1.98	-9.68×10^{-3}	-3.7×10^{-2}	.11	2.1×10^{-7}	.86

TABLE 6b. $\varepsilon_r = A + Bt^m$

Sample	σ (Kb)	P_c (Kb)	A	B	m	MSR	R^2
46A	2.52	.1	9.7×10^{-4}	3.06×10^{-3}	.12	5.4×10^{-9}	.99
44A	3.18	.25	2.7×10^{-3}	4.09×10^{-3}	.05	2.0×10^{-8}	.95
7A	3.95	.53	2.93×10^{-3}	3.76×10^{-3}	.05	7.0×10^{-9}	.99
9A	4.1	.53	2.95×10^{-3}	1.32×10^{-3}	.14	2.2×10^{-8}	.97
10A	4.13	.53	3.35×10^{-3}	9.31×10^{-4}	.12	2.9×10^{-9}	.99
12A	4.22	.55	3.67×10^{-3}	4.22×10^{-4}	.23	5.9×10^{-8}	.97
13A	4.31	.55	2.62×10^{-3}	1.41×10^{-3}	.12	6.7×10^{-9}	.99
14A	4.4	.53	1.52×10^{-3}	3.81×10^{-3}	.1	3.5×10^{-9}	.99
15A	4.5	.54	3.62×10^{-3}	1.48×10^{-2}	.19	4.3×10^{-9}	.99
16A	4.6	.53	1.9×10^{-3}	4.95×10^{-2}	.14	4.8×10^{-9}	.99
18A	5.4	1.0	4.88×10^{-3}	5.03×10^{-4}	.33	8.9×10^{-9}	.98
27B	5.5	1.01	4.56×10^{-3}	2.13×10^{-3}	.25	1.7×10^{-8}	.98
26B	5.55	1.01	4.89×10^{-3}	1.15×10^{-2}	.15	4.3×10^{-9}	.99
29B	5.75	1.02	5.76×10^{-3}	5.20×10^{-3}	.32	7.3×10^{-9}	.99
30B	5.9	1.0	6.18×10^{-3}	5.87×10^{-4}	.25	6.9×10^{-9}	.98
34B	7.6	1.98	8.42×10^{-3}	1.45×10^{-3}	.28	1.6×10^{-8}	.98
36B	7.75	1.98	6.69×10^{-3}	1.54×10^{-3}	.1	5.7×10^{-8}	.89
35B	7.9	1.98	4.48×10^{-3}	4.24×10^{-3}	.1	8.8×10^{-8}	.95

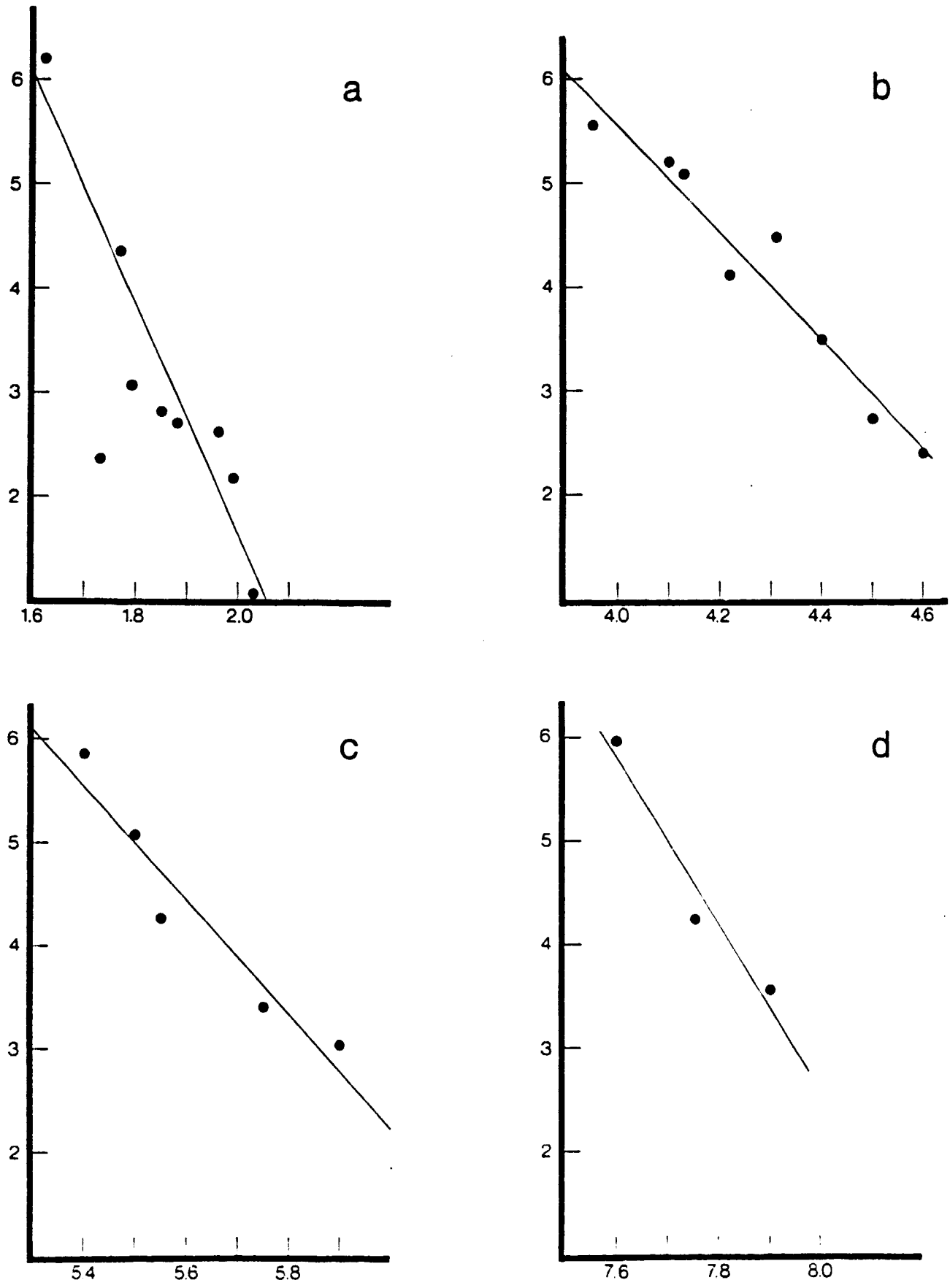

Figure 2

FIGURE CAPTIONS

Figure 1. Stress difference at failure as a function of confining pressure for fast loading (100 bars sec^{-1}) fracture tests.

Figure 2. Logarithm of the failure time in seconds (y axis) vs. stress difference in kilobars (x axis) at confining pressures of (a) 1 bar, (b) 530 bars, (c), 1000 bars, and (d) 2000 bars. Best fit, least-squares regression line is shown.

Figure 3. Inelastic volumetric strains at stress differences normalized to the fracture strength at each pressure. Solid symbols are Δ_2 at the onset of tertiary creep (from Table 2), open symbols are Δ prior to failure (from Table 1).

Figure 4. Dilatant volumetric strain at the onset of the instability leading to failure as a function of pressure. Open symbols are for constant-rate fracture tests, closed symbols for creep tests. Error bars are standard deviations.

Figure 5. Histograms of crack length and angle spectra for samples subjected to 1 bar, 530 bars and 1000 bars at 87% of the corresponding fracture strength. Each unit represents one crack within a 5 $\mu m \times 30^{\circ}$ slot. One hundred representative cracks are shown in each histogram.

Figure 6. Log of the failure time as a function of the applied load normalized to the short-term breaking strength at the corresponding pressure. WG is for water saturated Westerly granite [Wawersik, 1972]. Because of loading rate differences, to be strictly comparable, the WG curve should be shifted downwards about 2 orders of magnitude in time. Symbols are the same as in Figure 3.

Figure 7. Rupture times expected under various maximum and minimum stress states. Isochrons are based on extrapolation of equation 6 using the parameters listed in Table 3.

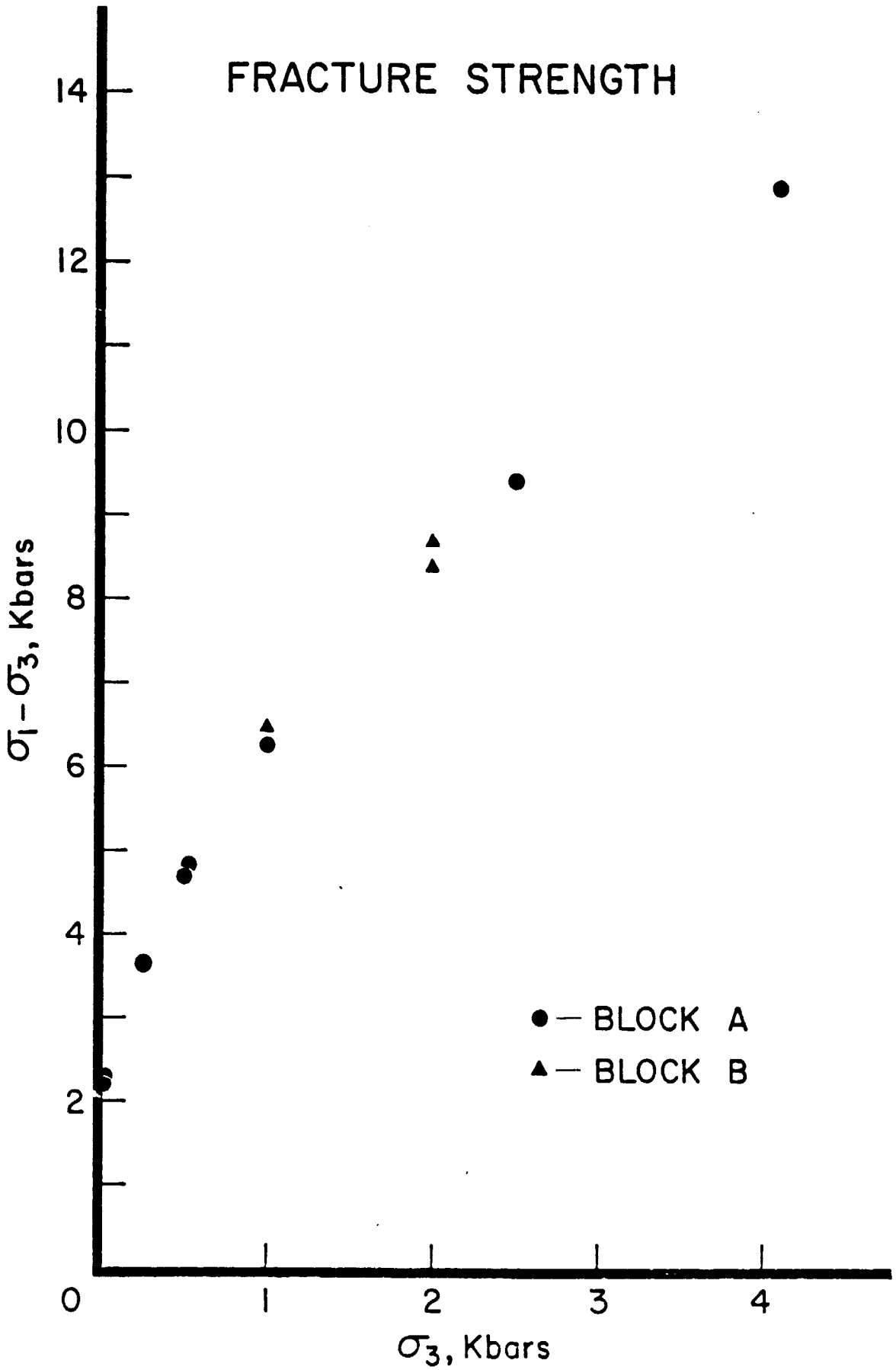
FRACTURE STRENGTH
14
12
10
8
6
4
2
0
1
2
3
4
$\sigma_1 - \sigma_3$, Kbars
σ_3, Kbars
● — BLOCK A
▲ — BLOCK B

Figure 1

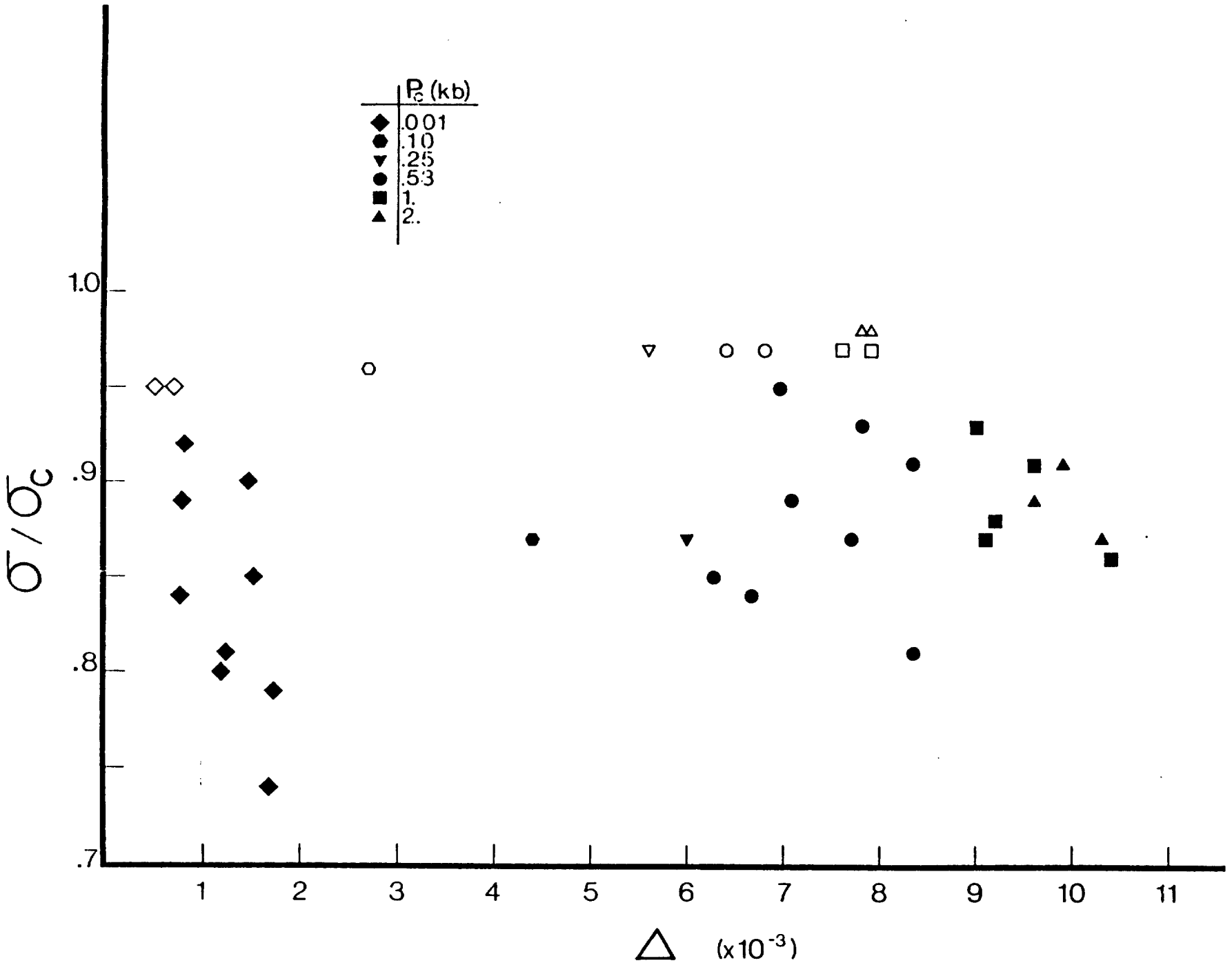
P_c (kb)
.001
.10
.25
.53
1.
2.
1.0
.9
.8
.7
σ / σ_c
1
2
3
4
5
6
7
8
9
10
11
Δ ($\times 10^{-3}$)

Figure 3

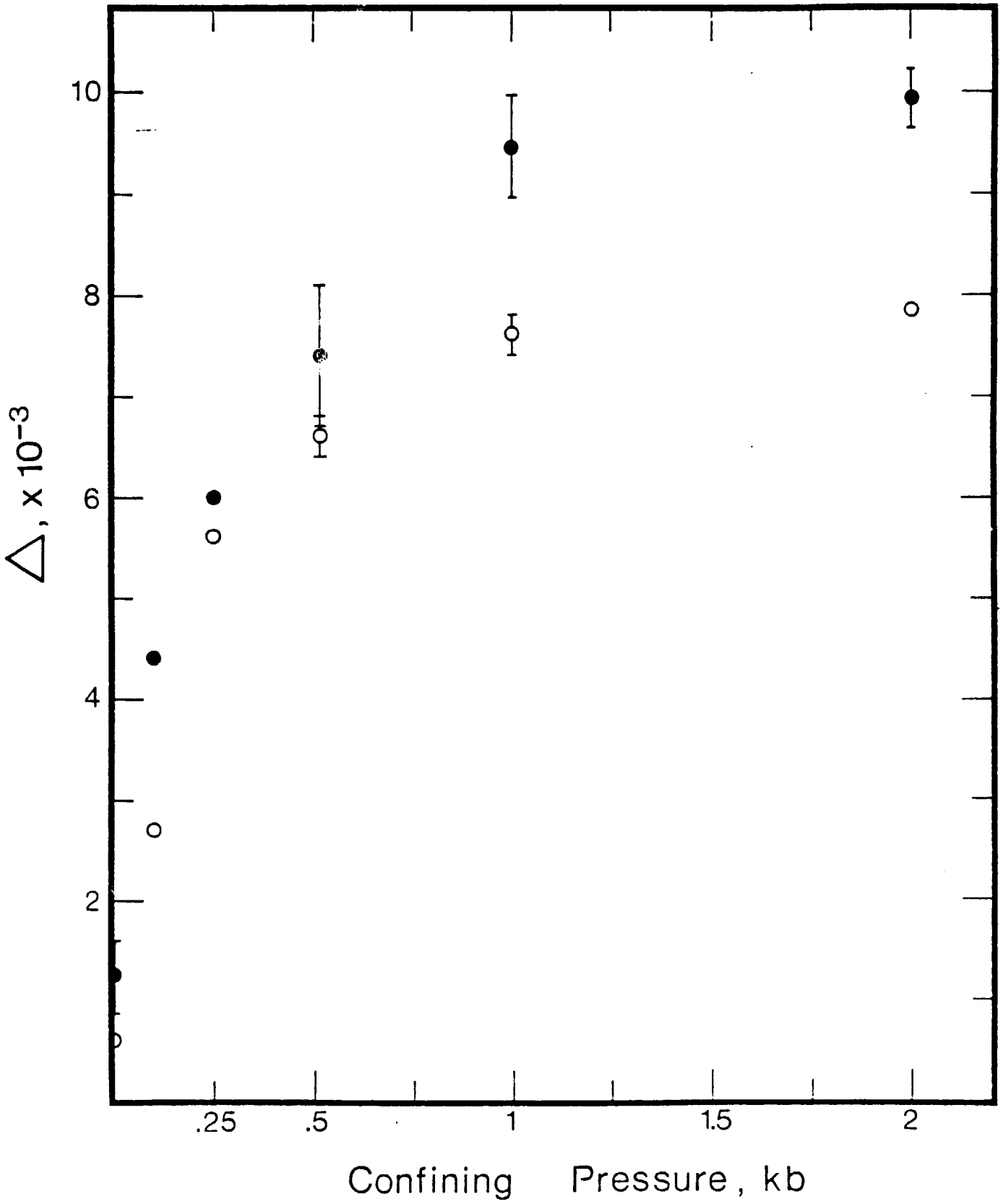

Figure 4

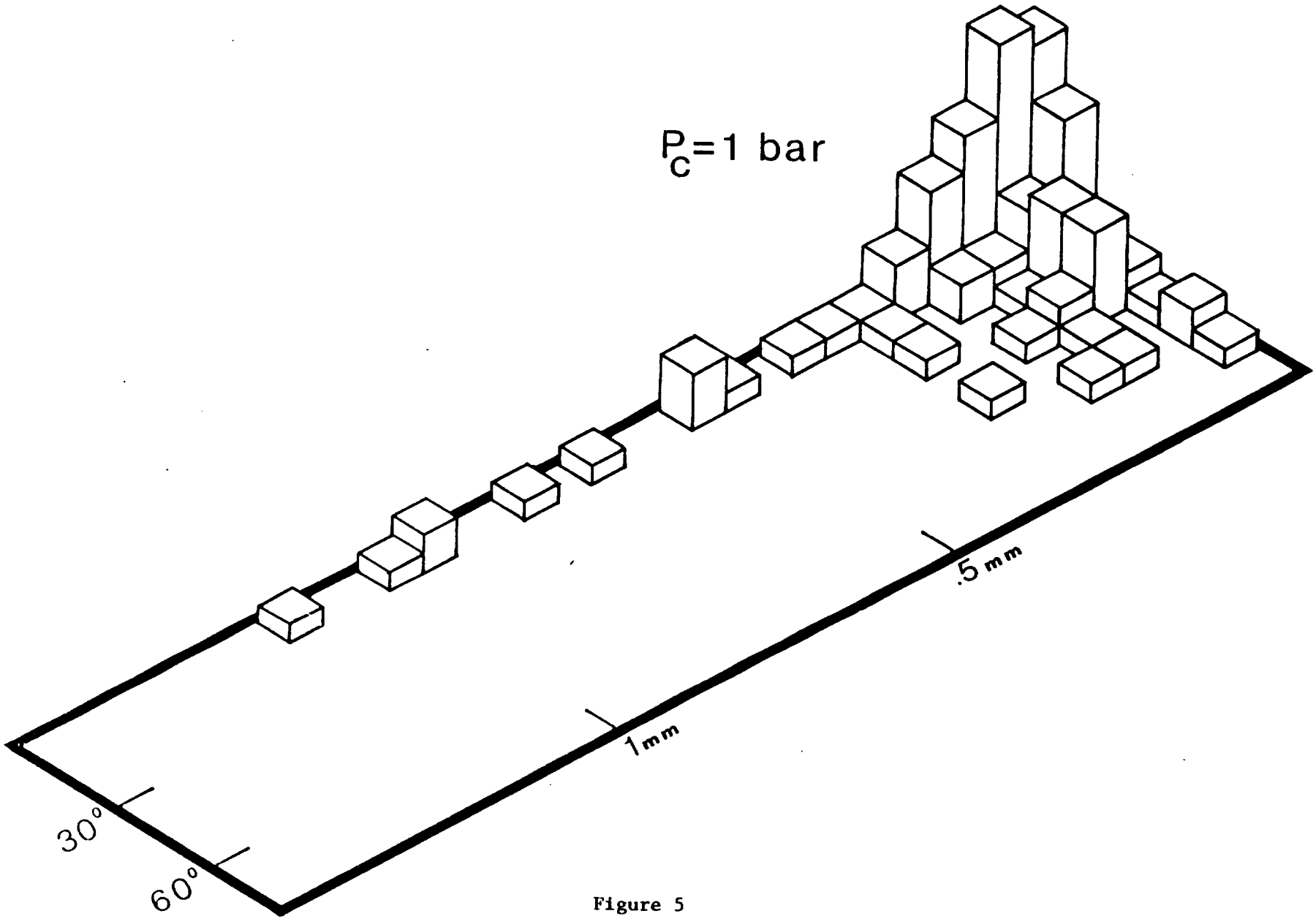

Figure 5

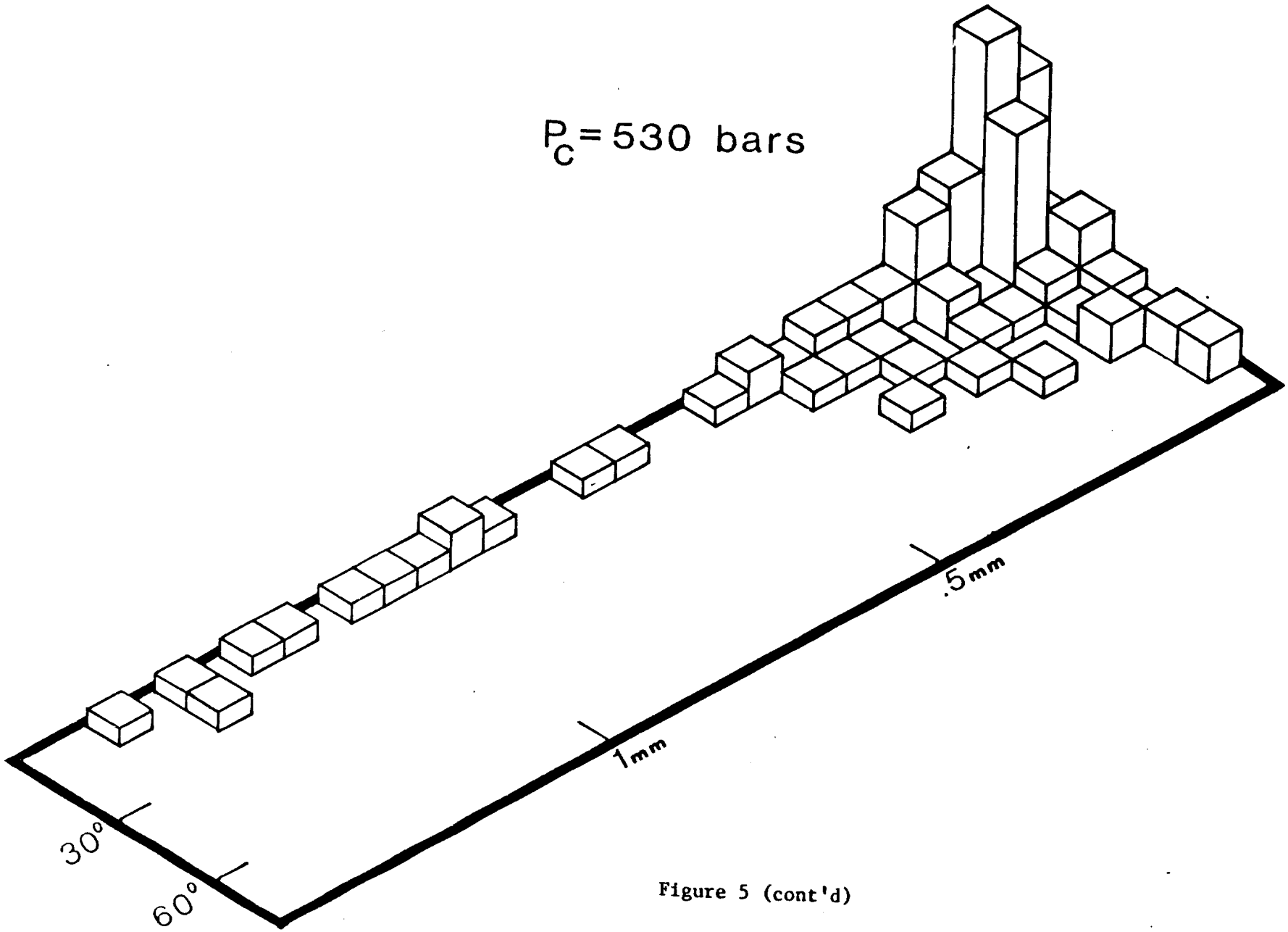

Figure 5 (cont'd)

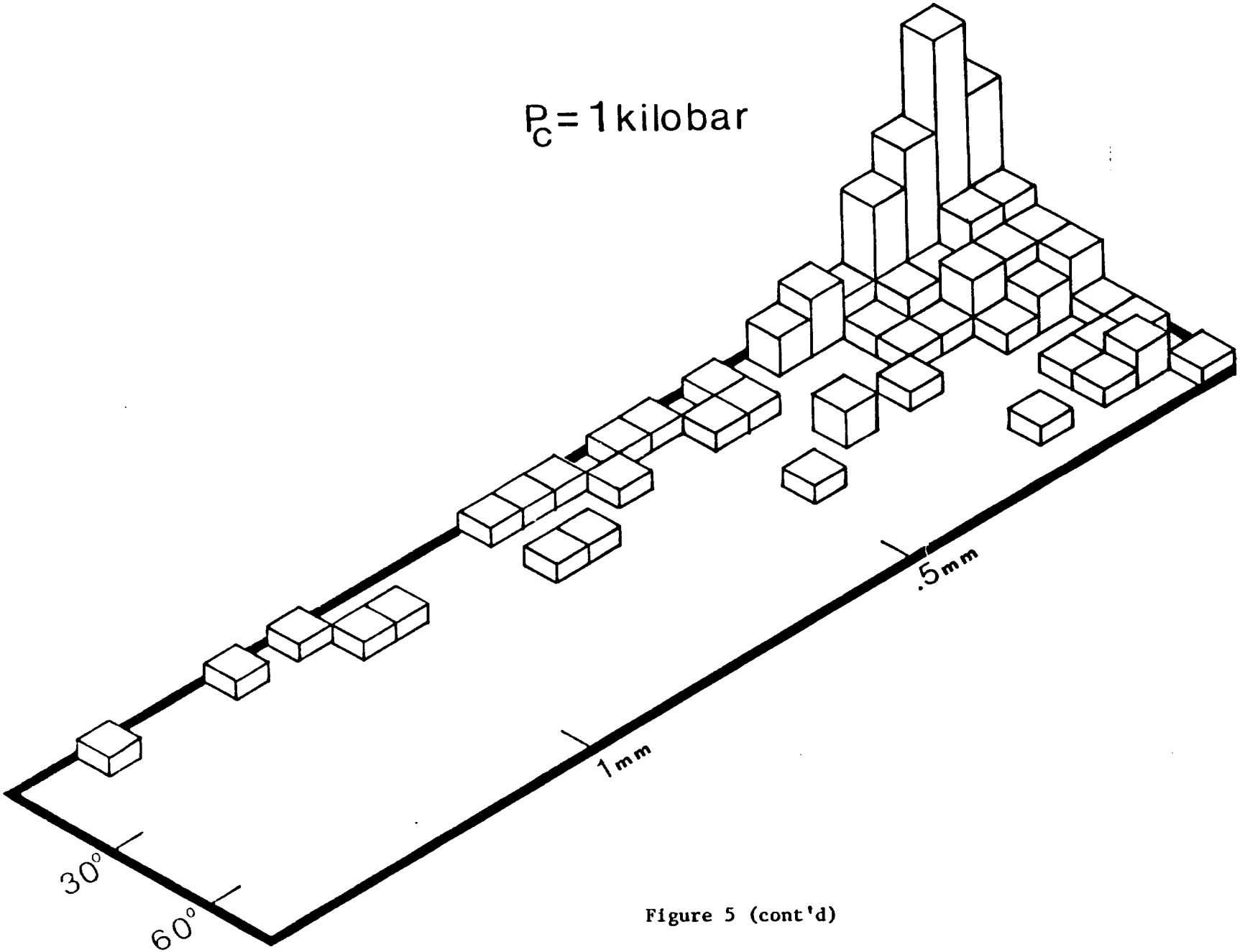

Figure 5 (cont'd)

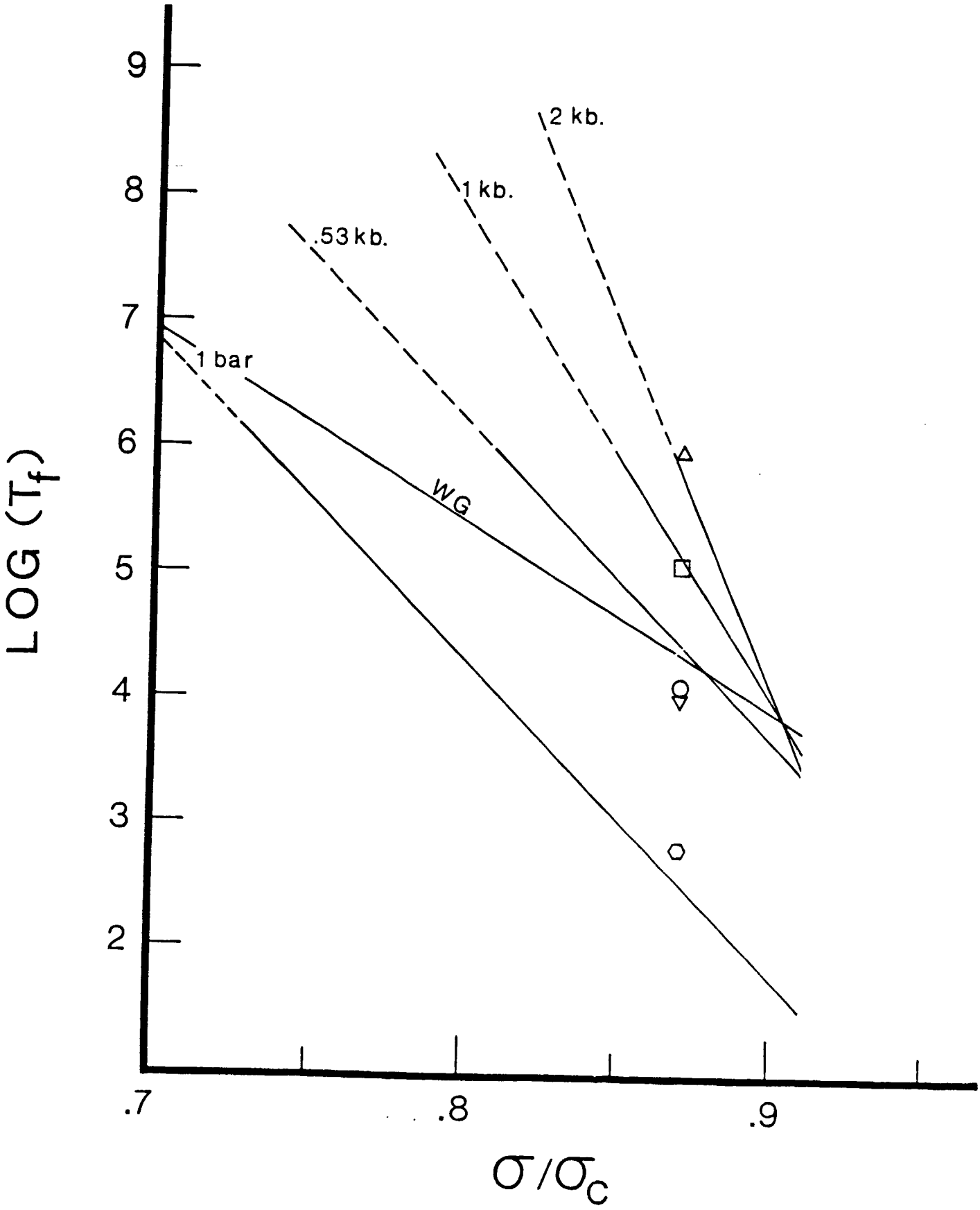

Figure 6

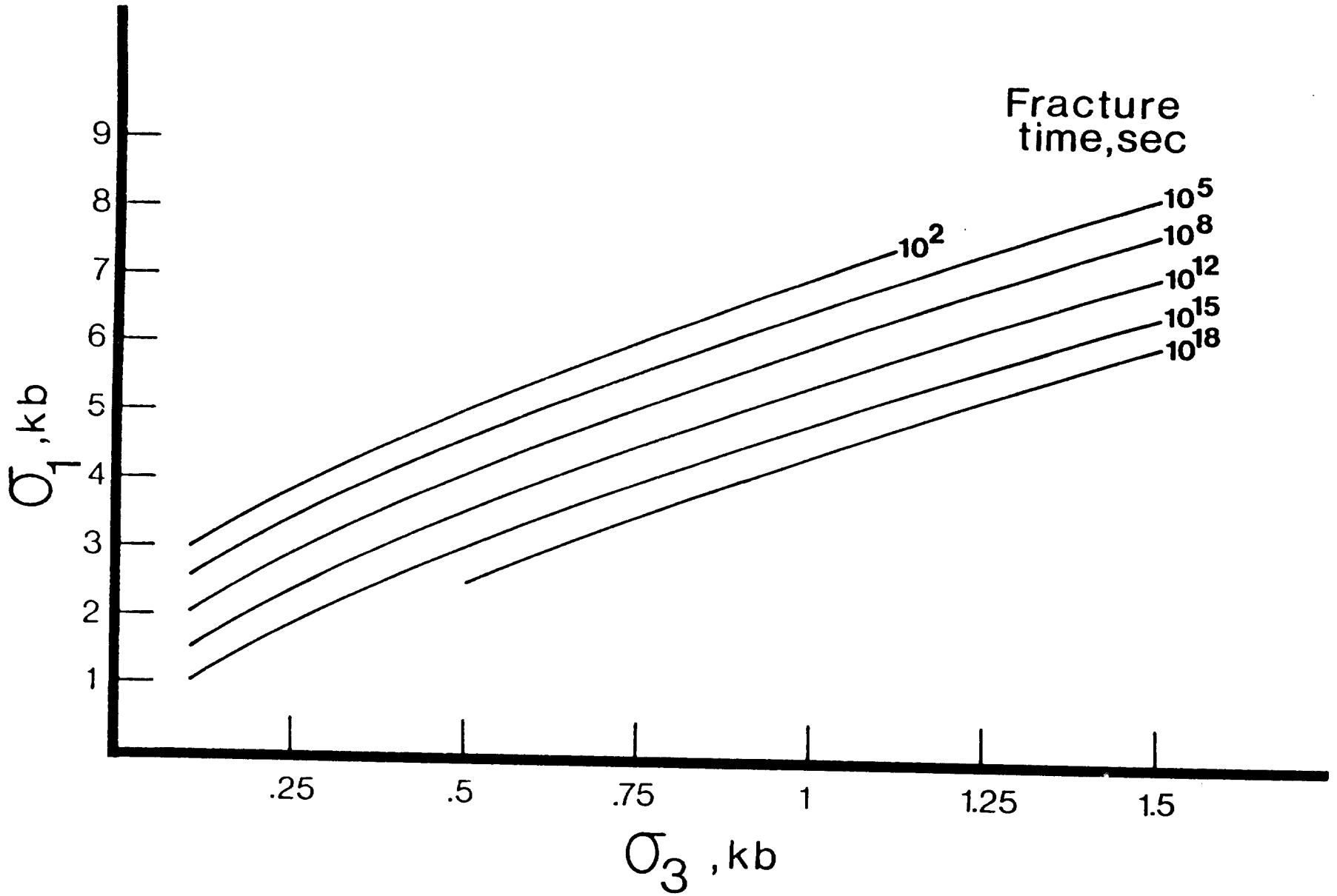
Fracture
time,sec
10^5
10^8
10^{12}
10^{15}
10^{18}
10^2
9
8
7
6
5
4
3
2
1
σ_1, kb
.25
.5
.75
1
1.25
1.5
σ_3, kb

Figure 7